Photonic “hourglass” design for efficient quantum light emission

Østerkryger, Andreas Dyhl; Claudon, Julien; Gérard, Jean Michel; Gregersen, Niels

Published in:
Optics Letters

Link to article, DOI:
10.1364/OL.44.002617

Publication date:
2019

Document Version
Peer reviewed version

A photonic "hourglass" design for efficient quantum light emission

ANDREAS DYHL OSTERKRYGER[1], JULIEN CLAUDON[2], JEAN-MICHEL GÉRARD[2], AND NIELS GREGERSEN[1,*]

[1] DTU Fotonik, Department of Photonics Engineering, Technical University of Denmark, DK-2800 Kongens Lyngby, Denmark
[2] Univ. Grenoble Alpes, CEA, INAC, PHELIQS, "Nanophysique et semiconducteurs" group, F-38000 Grenoble, France
[*] Corresponding author: ngre@fotonik.dtu.dk

Compiled April 22, 2019

We propose a novel "hourglass"-shaped design for highly efficient generation and collection of quantum light. The design features a quantum dot in a photonic nanowire sandwiched between tapered Bragg reflectors. For a Purcell factor of 9, the design features a spontaneous emission coupling of 0.993 to the cavity mode enabled by the strong dielectric screening of radiation modes. Thanks to a highly reflecting bottom mirror, we furthermore demonstrate a collection efficiency of 0.95 to a Gaussian profile. Finally, this photonic structure features a broad operation bandwidth, as large as 11 nm.

OCIS codes: (140.3300) Laser beam shaping; (140.3948) Microcavity devices; (250.5590) Quantum-well, -wire and -dot devices.

http://dx.doi.org/10.1364/ao.XX.XXXXXX

Within optical quantum information technology [1], a key component is the quantum light source capable of emitting single photons and entangled photon pairs (EPPs) on demand. For scalable information processing, the source must feature both near-unity extraction efficiency and photon indistinguishability. For several decades, spontaneous parametric down-conversion [2] has been a workhorse for quantum light generation, however its probabilistic nature leads to efficiencies of only a few percent. On the other hand, the semiconductor quantum dot (QD) embedded in a structured environment [3] has in recent years emerged as a promising platform for realizing deterministic single-photon [4] and EPP sources [5]. Today, the most successful design strategy for single-photon generation is based on a QD in a microcavity pillar [6, 7], where Purcell enhancement is exploited to ensure high efficiency. Here, a photon collection efficiency ε up to 0.79 [8] has been demonstrated, and more recently an ε of 0.66 combined with 0.985 photon indistinguishability [9] was reported. However, the micropillar design approach is inherently narrowband (bandwidth $\Delta\lambda \sim 0.2$ nm), whereas EPP generation using the exciton-biexciton cascade requires a bandwidth of typically a few nm. While EPP generation from a double-pillar "molecule" geometry [10] with an extraction efficiency ε of 0.35 has been demonstrated, this design suffers from a highly non-Gaussian far-field emission pattern. An alternative design approach consists in placing the QD in a photonic nanowire, where a dielectric screening effect [11] is employed to ensure high efficiency. In particular, no resonant effect is used and the design approach is thus broadband. Single-photon generation efficiency ε up to 0.75 from "needle" [12] and "trumpet" nanowires [13–15] has been demonstrated as well as EPP generation [16, 17] with ε of 0.15. However, obtaining high photon indistinguishability from photonic nanowires remains a challenge. Known decoherence mechanisms include fast exciton energy fluctuations due to an unstable electrostatic environment [18] and well as interaction with phonons [19] and discrete vibration modes of the nanowire [20]. While resonant effects are not needed for high efficiency, it is nevertheless desirable to enhance the spontaneous emission (SE) rate to overcome [19] these decoherence mechanisms and ensure high indistinguishability. To this purpose it was recently suggested to introduce weak cavity effects by implementing a distributed Bragg reflector (DBR) in the "trumpet" taper [21]. Here the cavity consists of a bottom silica-gold mirror [22] and the top DBR. A bottleneck of this design is the bottom metal mirror with reflectivity limited to ~ 0.91 [21–23]. In particular, when the SE is Purcell enhanced in the presence of the DBR, this occurs at the cost of reduced efficiency due to increased light absorption in the metal.

To avoid this trade-off and to pave the way towards combined near-unity efficiency and indistinguishability, we propose in this Letter the "hourglass" design illustrated in Fig. 1(a). Its novelty consists of the combination of a top "trumpet" taper featuring a DBR [21] and a bottom inverted "trumpet" taper featuring another DBR [24] allowing for near-unity bottom mirror reflectivity. We will show that the "hourglass" may overcome the trade-offs of present design strategies both in terms of efficiency and indistinguishability [25]. In the following, we first discuss the single-mode model used to analyze the performance of the "hourglass". Subsequently, we discuss the achievable reflectivity of the bottom DBR mirror. After having fixed a geometry, we then present calculations of the Purcell factor F_P, the cavity coupling factor β_c, the collection efficiency ε and the bandwidth $\Delta\lambda$. We will demonstrate that the "hourglass" allows for an ε of 0.95 combined with a $\Delta\lambda$ of 11 nm and an F_P of 9. Finally, we discuss strategies for further increasing the efficiency towards unity.

In this Letter, we consider a rotationally symmetric structure suitable for the EPP application. The radius at the position of the

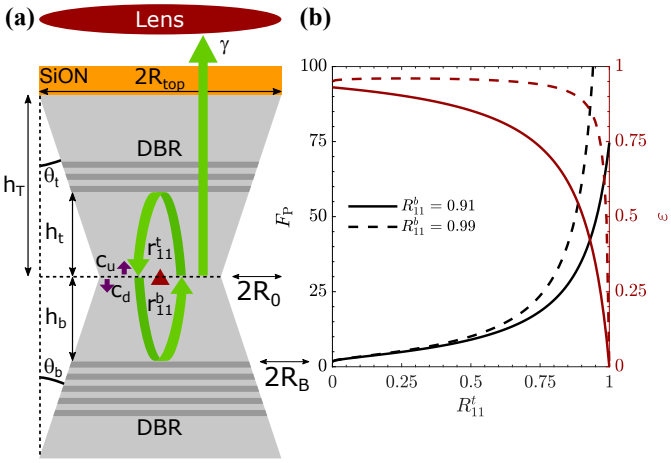

Fig. 1. (a) The "hourglass" design. (b) Purcell enhancement and total efficiency calculated using a single-mode model as function of the top mirror reflectivity for $R_{11}^{\mathrm{b}} = 0.91$ (solid) and $R_{11}^{\mathrm{b}} = 0.99$ (dashed). The parameters used are $\gamma = 0.975(1 - R_{11}^{t})$, $\Gamma_{\mathrm{HE}_{11}} = 0.88\Gamma_0$ and $\Gamma_{\mathrm{Rad}} = 0.04\Gamma_0$ [21].

QD is chosen as $R_0 = 0.114$ μm to ensure good coupling from the QD to the fundamental waveguide mode for our design wavelength $\lambda_{\mathrm{d}} = 925$ nm as discussed below. The cavity is formed by double "trumpets" with GaAs/AlGaAs DBRs featuring linear tapering profiles with side wall angles θ_{b} and θ_{t} and QD-DBR separation distances h_{b} and h_{t}. The thickness of the DBR layers is optimized using the procedure outlined in Appendix C of Ref. [21]. In addition, the design features a silicon oxynitride (SiON) [26] anti-reflecting (AR) coating. The refractive indices are those of Ref. [21] except for the AR coating for which we have chosen $\sqrt{n_{\mathrm{GaAs}}}$. In the following, we investigate a symmetric structure such that $\theta_{\mathrm{b}} = \theta_{\mathrm{t}} \equiv \theta$ and $h_{\mathrm{b}} = h_{\mathrm{t}} \equiv h$. The numerical simulations are performed using a Fourier modal method [27] with a true open geometry boundary condition combined with a standard scattering matrix formalism [28].

We present results both from exact calculations using a full model as well as from the single-mode model of Ref. [21], which is restated here for clarity. We consider the propagation of the fundamental guided HE_{11} mode in the different sections of the "hourglass" structure as sketched in Fig. 1(a). We start by considering an infinitely long uniform wire. Here, the fraction of QD SE funnelled into the guided mode is $\beta_{\mathrm{g}} \equiv \Gamma_{\mathrm{HE}_{11}}/(\Gamma_{\mathrm{HE}_{11}} + \Gamma_{\mathrm{Rad}})$, where $\Gamma_{\mathrm{HE}_{11}}$ (Γ_{Rad}) is the SE rate into the HE_{11} mode (radiation modes) of the uniform nanowire. β_{g} reaches a maximum of 0.96 [21] for a wire radius $R_0 = 114$ nm. We now consider the full "hourglass" geometry, where we define $c_{u(d)}$ as the complex amplitude coefficient of the fundamental upward (downward) propagating mode given by

$$c_{\mathrm{u}} = c_0 \frac{1 + r_{11}^{\mathrm{b}}}{1 - r_{11}^{\mathrm{b}} r_{11}^{\mathrm{t}}}, \qquad c_{\mathrm{d}} = c_0 \frac{1 + r_{11}^{\mathrm{t}}}{1 - r_{11}^{\mathrm{b}} r_{11}^{\mathrm{t}}}, \tag{1}$$

where $c_0 = \sqrt{\Gamma_{\mathrm{HE}_{11}}/2}$ is the HE_{11} amplitude coefficient for an infinitely long nanowire, and r_{11}^{b} and r_{11}^{t} are complex modal reflection coefficients of the bottom and top mirrors, respectively, including propagation phases between the QD and the first AlGaAs layer. The total SE rate Γ_{T} of the full geometry is then computed as

$$\Gamma_{\mathrm{T}} = \left(1 - |r_{11}^{\mathrm{t}}|^2\right) |c_{\mathrm{u}}|^2 + \left(1 - |r_{11}^{\mathrm{b}}|^2\right) |c_{\mathrm{d}}|^2 + \Gamma_{\mathrm{Rad}}, \tag{2}$$

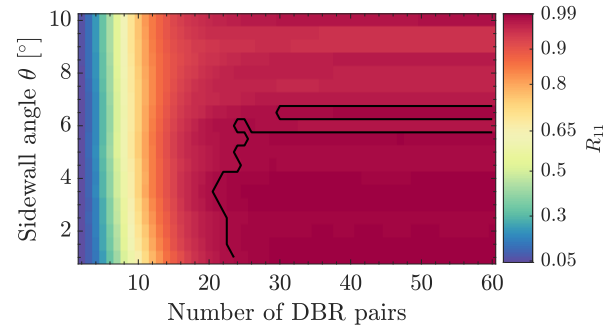

Fig. 2. Bottom mirror reflectivity R_{11}^{b} as function of number of DBR pairs and sidewall angle θ. The first DBR layer is placed at a distance h_{b} below the QD, such that the radius of the first DBR layer is $R_{\mathrm{B}} = 150$ nm. The black contour line indicates 0.98 reflectivity.

and furthermore we define a *generalized* Purcell factor as

$$F_{\mathrm{P}} = \mathrm{Re}\left[\frac{(1 + r_{11}^{\mathrm{t}})(1 + r_{11}^{\mathrm{b}})}{1 - r_{11}^{\mathrm{t}} r_{11}^{\mathrm{b}}}\right] \frac{\Gamma_{\mathrm{HE}_{11}}}{\Gamma_0}, \tag{3}$$

where Γ_0 is the bulk SE rate. This generalized Purcell factor should be understood as the local density of states at the position of the emitter and correctly describes the normalized SE rate into the cavity mode not only at resonance but at all wavelengths as discussed in detail in Ref. [21]. The cavity SE coupling factor is defined using the Purcell factor as $\beta_{\mathrm{c}} = F_{\mathrm{P}}\Gamma_0/\Gamma_{\mathrm{T}}$. Finally, we define the efficiency ε as the ratio of the power coupled to a Gaussian mode in the far field [13, 14] collected using a lens with 0.8 numerical aperture. It is given by

$$\varepsilon = \gamma |c_{\mathrm{u}}|^2/\Gamma_{\mathrm{T}}, \tag{4}$$

where γ is the total transmission of the fundamental mode from the QD to the first lens including the overlap with a Gaussian profile [13, 14].

To understand the impact of a highly reflecting bottom mirror we present the collection efficiency (Eq. (4)) and the Purcell enhancement (Eq. (3)) as function of the top mirror reflectivity $R_{11}^{t} = |r_{11}^{t}|^2$ in Fig. 1(b) for bottom mirror reflectivities $R_{11}^{b} = |r_{11}^{b}|^2$ of 0.91 and 0.99. For a reflectivity of 0.91 corresponding to the silica-gold mirror, we observe a clear compromise between obtaining simultaneously high Purcell enhancement and high collection efficiency. However, for $R_{11}^{b} = 0.99$ we can obtain a Purcell factor above 20 without sacrificing collection efficiency. Clearly, the implementation of a bottom mirror with near-unity reflectivity is crucial in the pursuit of quantum light sources for scalable quantum information processing.

We now present the calculated modal reflectivity R_{11}^{b} of the tapered DBR bottom mirror as function of the sidewall angle θ and the number of DBR layer pairs in Fig. 2. Since the reflectivity of the DBR is significantly compromised for nanowire radii below $\sim 0.15\lambda$ [22], we have chosen to place the first DBR pair at a QD-DBR height h corresponding to a radius R_{B} of 150 nm. We observe that a reflectivity above 0.98 is achievable for a sidewall angle θ below 6°, and the general trend is that the reflectivity improves with decreasing angle and increasing number of layer pairs. Additionally, careful inspection reveals oscillations in the reflectivity as function of the sidewall angle. These oscillations are due to coupling between the fundamental mode and higher

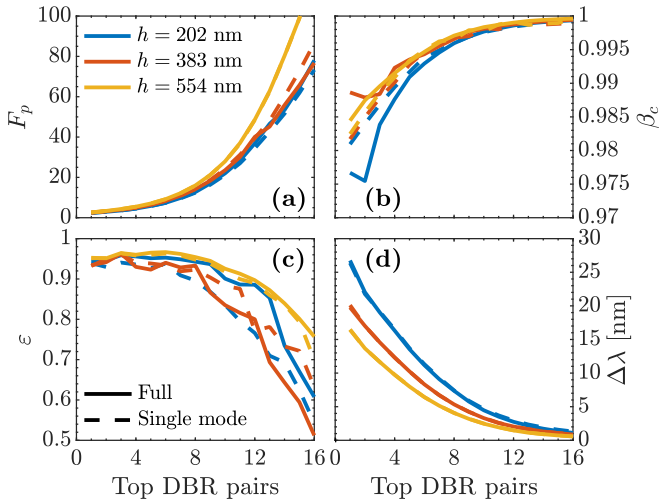

Fig. 3. Purcell enhancement F_P (a), cavity SE coupling factor β_c (b), collection efficiency ε (c) and bandwidth $\Delta\lambda$ of the Purcell enhancement (d) as function of the number of DBR pairs in the top mirror computed for the first three resonant QD-DBR separation distances using the full model (solid curves) and the single-mode model (dashed curves).

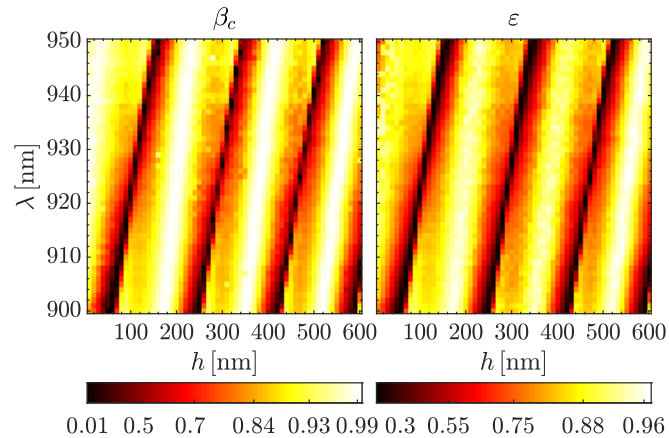

Fig. 4. Cavity coupling factor β_c and collection efficiency ε as function of emission wavelength λ and QD-DBR separation distance h with $\theta = 4.1°$, $R_{Top} = 1.2\,\mu$m, $h_T = 15\,\mu$m and 40 (6) layer pairs in the bottom (top) DBR.

order modes at the position of the first AlGaAs layer and could be suppressed by increasing R_B or by introducing an adiabatic DBR profile [29] with a gradually increasing AlGaAs layer thickness and/or a gradually decreasing AlGaAs refractive index.

A small sidewall angle θ is required for adiabatic propagation [23] of the HE_{11} mode through the taper, and a large top radius R_{Top} is needed to ensure a low output beam divergence [13–15] and a good coupling to a Gaussian mode in the far field. However, a large R_{Top} and a small θ lead to a large top taper height h_T, whereas a compact device is preferential for the fabrication. There is thus a trade-off between high performance and choosing an h_T compatible with practical fabrication constraints. In the following, we chose $h_T = 15\,\mu$m and $R_{Top} = 1.2\,\mu$m corresponding to a θ of 4.1°, which are parameters well compatible [15] with feasible fabrication. With this choice of parameters we compute a transmission γ of 0.975 to a Gaussian profile for the bare taper geometry, i.e. with no DBR in the top taper. Furthermore, we chose 40 layer pairs in the bottom DBR, which for R_B = 150 nm leads to a bottom reflectivity R^b_{11} of 0.987 - a remarkable improvement in reflectivity as compared to the dielectric-metal mirror. In the following, we investigate the influence of the number of layer pairs in the top DBR and of the QD-DBR separation h. The maximum Purcell enhancement occurs when the QD is positioned at an antinode of the cavity mode, which is the case for the discrete values of h for which the total phase $\arg(r^t_{11} r^b_{11})$ describing a cavity roundtrip is zero. We note that increasing the number of DBR layer pairs from 4 to 40 modifies the total phase by less than 0.5°, which justifies our choice of identical top and bottom QD-DBR separation distances.

We present the computed Purcell enhancement F_P, cavity coupling factor β_c, collection efficiency ε and bandwidth $\Delta\lambda$ of the Purcell enhancement in Fig. 3 as function of the number of top DBR layer pairs. The bandwidth is determined by computing the Q factor using the approach given in Ref. [30]. We present results for the first three separations h for which the emitter is located at an antinode at the design wavelength of λ_d = 925 nm. We observe that the Purcell factor increases slightly with larger separation h. As the trumpet radius increases, the HE_{11} modal overlap at the GaAs/AlGaAs interfaces is improved, and this in turn leads to increased reflectivity [21] and Purcell enhancement. The cavity coupling factor β_c exceeds 0.97 even for a weakly reflecting DBR, which is a result of dielectric screening by the nanowire [11]. The collection efficiency ε is slightly improved with h due to the increase in Purcell enhancement, and it remains above $\sim$ 0.9 for up to 8 layer pairs thanks to the high reflectivity of the bottom DBR. As expected the bandwidth is largest for the shortest cavity, for which we observe that a $\Delta\lambda$ of 11 nm is obtained for 6 layer pairs. Fig. 3 includes results obtained from the single-mode model described above as well as from a full model taking into account interaction of the HE_{11} mode with radiation modes in the evaluation of the amplitude coefficients c_u and c_d. Whereas the agreement for F_P and $\Delta\lambda$ for two models is good, discrepancies are observed for β_c and ε which increase with reduced QD-DBR separation h. This discrepancy originates from a modified c_u coefficient for the smaller cavities due to interaction with radiation modes. Whereas the single-mode model has provided remarkable agreement for simpler designs [23, 24], we conclude that full simulations are needed to predict the performance in the presence of significant cavity effects.

We now investigate the performance of an "hourglass" design featuring 40 (6) pairs in the bottom (top) DBR. The Purcell factor for this design is slightly larger than for the case with the silica-gold mirror [21] due to the increased reflectivity of the bottom DBR with a maximum F_P of $\sim$ 9 at the design wavelength and a corresponding β_c of 0.993. Furthermore, efficiencies ε of 0.95 and 0.965 are obtained for h = 202 and 554 nm respectively - significant improvements compared to the ε of 0.8 reported in Ref. [21]. While keeping the design wavelength λ_d = 925 nm fixed, we then present the cavity coupling factor β_c and the collection efficiency ε in Fig. 4 as function of emitter wavelength λ and QD-DBR separation distance h. We observe that a β_c above 0.95 is obtained over a 36 nm range for the first resonance line highlighting the broadband nature of the design in terms of efficient coupling to the cavity mode. This leads to a collection efficiency above 0.88 over the same range for h = 202 nm. Similarly, Fig. 4 demonstrates the good tolerance of β_c and ε with respect to h thus ensuring feasibility in the fabrication. Finally, we note that, for h = 202 nm, the 0.95 collection efficiency to a Gaussian mode

is combined with an 11 nm bandwidth, which makes the design attractive for the EPP application. The combination of the high Purcell factor with the broad spectral bandwidth is achieved thanks to a small cavity mode volume of $\sim 0.7\ (\lambda/n)^3$ [21].

Thus the "hourglass" design clearly has potential to outperform the micropillar geometry in the EPP application, and we now consider its strengths within the single-photon source application, where the micropillar geometry currently represents state-of-the-art. Here, the rotationally symmetric micropillar design suffers from lack of polarization control, which reduces its efficiency by a factor of 2 due to polarization filtering. An elliptical cross-section has been suggested [7] to establish polarization control, however it necessarily reduces the overlap to a Gaussian profile in the far field leading to a trade-off between degree of polarization and efficiency. On the other hand, the "hourglass" allows for an elliptical cross-section [31] at the position of the emitter combined with a rotationally symmetric top termination thus enabling for polarization control without compromising the far field pattern. Additionally, we note that the micropillar relies on Purcell enhancement to ensure high efficiency, and it is thus ultimately limited by a trade-off [25] between efficiency and indistinguishability in the presence of phonon-induced decoherence. Whereas calculations of the indistinguishability are beyond the scope of this Letter, we remark that the above trade-off is avoided in the "hourglass" design as high efficiency is obtained independently of the Purcell factor, which instead may be chosen to maximize the indistinguishability.

Whereas an exhaustive parameter optimization for the "hourglass" design is beyond the scope of this Letter, we finally now qualitatively point out strategies for increasing the efficiency further towards unity. Three main factors limit the collection efficiency of the present design: 1) A DBR operating in a low-diameter regime suffers from scattering [32] to higher order modes. As discussed above, this scattering can be suppressed using adiabatic engineering [29] of the layer thicknesses and of the refractive index profile. 2) The side wall angle θ of 4.1° can be reduced further to increase γ for the bare taper. The price to pay is an increased top taper height h_{T}. We have chosen a modest h_{T} of 15 μm, however top tapers of almost twice this height [15] have already been demonstrated experimentally. 3) The maximum overlap between a HE_{11} mode in a GaAs nanowire (Bessel profile) and an optical fibre (Gaussian profile) is 0.985. This limitation, which also applies to the micropillar, can be overcome by butt-coupling the source to a tapered optical fiber.

In conclusion, we have proposed an "hourglass"-shaped design for a highly efficient source of quantum light. For a modest taper height compatible with fabrication, we show that an efficiency of 0.95 is achievable combined with an 11 nm bandwidth. The design does not rely on Purcell enhancement to achieve high efficiency, and the Purcell factor can be freely chosen e.g. to maximize the photon indistinguishability.

Funding. QuantERA ERA-NET Cofund (HYPER-U-P-S); Innovation Fund Denmark (7074-00004B); Independent Research Fund Denmark (DFF-4181-00416); French National Research Agency (ANR-16-CE09-0010-01); CEA DRF Impulsion (SOUPAPE).

REFERENCES

1. S. Barz, J. Phys. B At. Mol. Opt. Phys. **48**, 083001 (2015).
2. P. G. Kwiat, K. Mattle, H. Weinfurter, A. Zeilinger, A. V. Sergienko, and Y. Shih, Phys. Rev. Lett. **75**, 4337 (1995).
3. P. Lodahl, S. Mahmoodian, and S. Stobbe, Rev. Mod. Phys. **87**, 347 (2015).
4. I. Aharonovich, D. Englund, and M. Toth, Nat. Photonics **10**, 631 (2016).
5. D. Huber, M. Reindl, J. Aberl, A. Rastelli, and R. Trotta, J. Opt. **20**, 073002 (2018).
6. S. Reitzenstein and A. Forchel, J. Phys. D. Appl. Phys. **43**, 033001 (2010).
7. E. Moreau, I. Robert, J. M. Gérard, I. Abram, L. Manin, and V. Thierry-Mieg, Appl. Phys. Lett. **79**, 2865 (2001).
8. O. Gazzano, S. Michaelis de Vasconcellos, C. Arnold, A. Nowak, E. Galopin, I. Sagnes, L. Lanco, A. Lemaître, and P. Senellart, Nat. Commun. **4**, 1425 (2013).
9. X. Ding, Y. He, Z.-C. Duan, N. Gregersen, M.-C. Chen, S. Unsleber, S. Maier, C. Schneider, M. Kamp, S. Höfling, C.-Y. Lu, and J.-W. Pan, Phys. Rev. Lett. **116**, 020401 (2016).
10. A. Dousse, J. Suffczyński, A. Beveratos, O. Krebs, A. Lemaître, I. Sagnes, J. Bloch, P. Voisin, and P. Senellart, Nature. **466**, 217 (2010).
11. J. Bleuse, J. Claudon, M. Creasey, N. S. Malik, J.-M. Gérard, I. Maksymov, J.-P. Hugonin, and P. Lalanne, Phys. Rev. Lett. **106**, 103601 (2011).
12. J. Claudon, J. Bleuse, N. S. Malik, M. Bazin, P. Jaffrennou, N. Gregersen, C. Sauvan, P. Lalanne, and J.-M. Gérard, Nat. Photonics **4**, 174 (2010).
13. M. Munsch, N. S. Malik, E. Dupuy, A. Delga, J. Bleuse, J.-M. Gérard, J. Claudon, N. Gregersen, and J. Mørk, Phys. Rev. Lett. **110**, 177402 (2013).
14. M. Munsch, N. S. Malik, E. Dupuy, A. Delga, J. Bleuse, J.-M. Gérard, J. Claudon, N. Gregersen, and J. Mørk, Phys. Rev. Lett. **111**, 239902 (2013).
15. P. Stepanov, A. Delga, N. Gregersen, E. Peinke, M. Munsch, J. Teissier, J. Mørk, M. Richard, J. Bleuse, J.-M. Gérard, and J. Claudon, Appl. Phys. Lett. **107**, 141106 (2015).
16. T. Huber, A. Predojević, M. Khoshnegar, D. Dalacu, P. J. Poole, H. Majedi, and G. Weihs, Nano Lett. **14**, 7107 (2014).
17. M. A. M. Versteegh, M. E. Reimer, K. D. Jöns, D. Dalacu, P. J. Poole, A. Gulinatti, A. Giudice, and V. Zwiller, Nat. Commun. **5**, 5298 (2014).
18. A. Berthelot, I. Favero, G. Cassabois, C. Voisin, C. Delalande, P. Roussignol, R. Ferreira, and J.-M. Gérard, Nat. Phys. **2**, 759 (2006).
19. P. Kaer, N. Gregersen, and J. Mørk, New J. Phys. **15**, 035027 (2013).
20. M. Munsch, A. V. Kuhlmann, D. Cadeddu, J.-M. Gérard, J. Claudon, M. Poggio, and R. J. Warburton, Nat. Commun. **8**, 76 (2017).
21. N. Gregersen, D. P. S. McCutcheon, J. Mørk, J.-M. Gérard, and J. Claudon, Opt. Express **24**, 20904 (2016).
22. I. Friedler, P. Lalanne, J. P. Hugonin, J. Claudon, J. M. Gérard, A. Beveratos, and I. Robert-Philip, Opt. Lett. **33**, 2635 (2008).
23. N. Gregersen, T. R. Nielsen, J. Mørk, J. Claudon, and J.-M. Gérard, Opt. Express **18**, 21204 (2010).
24. I. Friedler, C. Sauvan, J. P. Hugonin, P. Lalanne, J. Claudon, and J. M. Gérard, Opt. Express **17**, 2095 (2009).
25. J. Iles-Smith, D. P. S. McCutcheon, A. Nazir, and J. Mørk, Nat. Photonics **11**, 521 (2017).
26. R. Machorro, E. Samano, G. Soto, F. Villa, and L. Cota-Araiza, Mater. Lett. **45**, 47 (2000).
27. T. Häyrynen, J. R. de Lasson, and N. Gregersen, J. Opt. Soc. Am. A **33**, 1298 (2016).
28. A. V. Lavrinenko, J. Lægsgaard, N. Gregersen, F. Schmidt, and T. Søndergaard, "Numerical Methods in Photonics," (CRC Press, 2015), chap. 6, pp. 139–195.
29. M. Lermer, N. Gregersen, F. Dunzer, S. Reitzenstein, S. Höfling, J. Mørk, L. Worschech, M. Kamp, and A. Forchel, Phys. Rev. Lett. **108**, 057402 (2012).
30. N. Gregersen, S. Reitzenstein, C. Kistner, M. Strauss, C. Schneider, S. Höfling, L. Worschech, A. Forchel, T. R. Nielsen, J. Mørk, and J.-M. Gérard, IEEE J. Quantum Electron. **46**, 1470 (2010).
31. M. Munsch, J. Claudon, J. Bleuse, N. S. Malik, E. Dupuy, J.-M. Gérard, Y. Chen, N. Gregersen, and J. Mørk, Phys. Rev. Lett. **108**, 077405 (2012).
32. P. Lalanne, J. P. Hugonin, and J. M. Gérard, Appl. Phys. Lett. **84**, 4726 (2004).

FULL REFERENCES

1. S. Barz, "Quantum computing with photons: introduction to the circuit model, the one-way quantum computer, and the fundamental principles of photonic experiments," J. Phys. B At. Mol. Opt. Phys. **48**, 083001 (2015).
2. P. G. Kwiat, K. Mattle, H. Weinfurter, A. Zeilinger, A. V. Sergienko, and Y. Shih, "New High-Intensity Source of Polarization-Entangled Photon Pairs," Phys. Rev. Lett. **75**, 4337–4341 (1995).
3. P. Lodahl, S. Mahmoodian, and S. Stobbe, "Interfacing single photons and single quantum dots with photonic nanostructures," Rev. Mod. Phys. **87**, 347–400 (2015).
4. I. Aharonovich, D. Englund, and M. Toth, "Solid-state single-photon emitters," Nat. Photonics **10**, 631–641 (2016).
5. D. Huber, M. Reindl, J. Aberl, A. Rastelli, and R. Trotta, "Semiconductor quantum dots as an ideal source of polarization-entangled photon pairs on-demand: a review," J. Opt. **20**, 073002 (2018).
6. S. Reitzenstein and A. Forchel, "Quantum dot micropillars," J. Phys. D. Appl. Phys. **43**, 033001 (2010).
7. E. Moreau, I. Robert, J. M. Gérard, I. Abram, L. Manin, and V. Thierry-Mieg, "Single-mode solid-state single photon source based on isolated quantum dots in pillar microcavities," Appl. Phys. Lett. **79**, 2865–2867 (2001).
8. O. Gazzano, S. Michaelis de Vasconcellos, C. Arnold, A. Nowak, E. Galopin, I. Sagnes, L. Lanco, A. Lemaître, and P. Senellart, "Bright solid-state sources of indistinguishable single photons," Nat. Commun. **4**, 1425 (2013).
9. X. Ding, Y. He, Z.-C. Duan, N. Gregersen, M.-C. Chen, S. Unsleber, S. Maier, C. Schneider, M. Kamp, S. Höfling, C.-Y. Lu, and J.-W. Pan, "On-Demand Single Photons with High Extraction Efficiency and Near-Unity Indistinguishability from a Resonantly Driven Quantum Dot in a Micropillar," Phys. Rev. Lett. **116**, 020401 (2016).
10. A. Dousse, J. Suffczyński, A. Beveratos, O. Krebs, A. Lemaître, I. Sagnes, J. Bloch, P. Voisin, and P. Senellart, "Ultrabright source of entangled photon pairs," Nature. **466**, 217–220 (2010).
11. J. Bleuse, J. Claudon, M. Creasey, N. S. Malik, J.-M. Gérard, I. Maksymov, J.-P. Hugonin, and P. Lalanne, "Inhibition, enhancement, and control of spontaneous emission in photonic nanowires," Phys. Rev. Lett. **106**, 103601 (2011).
12. J. Claudon, J. Bleuse, N. S. Malik, M. Bazin, P. Jaffrennou, N. Gregersen, C. Sauvan, P. Lalanne, and J.-M. Gérard, "A highly efficient single-photon source based on a quantum dot in a photonic nanowire," Nat. Photonics **4**, 174–177 (2010).
13. M. Munsch, N. S. Malik, E. Dupuy, A. Delga, J. Bleuse, J.-M. Gérard, J. Claudon, N. Gregersen, and J. Mørk, "Dielectric GaAs antenna ensuring an efficient broadband coupling between an InAs quantum dot and a Gaussian optical beam," Phys. Rev. Lett. **110**, 177402 (2013).
14. M. Munsch, N. S. Malik, E. Dupuy, A. Delga, J. Bleuse, J.-M. Gérard, J. Claudon, N. Gregersen, and J. Mørk, "Erratum: Dielectric GaAs Antenna Ensuring an Efficient Broadband Coupling between an InAs Quantum Dot and a Gaussian Optical Beam [Phys. Rev. Lett. 110, 177402 (2013)]," Phys. Rev. Lett. **111**, 239902 (2013).
15. P. Stepanov, A. Delga, N. Gregersen, E. Peinke, M. Munsch, J. Teissier, J. Mørk, M. Richard, J. Bleuse, J.-M. Gérard, and J. Claudon, "Highly directive and Gaussian far-field emission from "giant" photonic trumpets," Appl. Phys. Lett. **107**, 141106 (2015).
16. T. Huber, A. Predojević, M. Khoshnegar, D. Dalacu, P. J. Poole, H. Majedi, and G. Weihs, "Polarization Entangled Photons from Quantum Dots Embedded in Nanowires," Nano Lett. **14**, 7107–7114 (2014).
17. M. A. M. Versteegh, M. E. Reimer, K. D. Jöns, D. Dalacu, P. J. Poole, A. Gulinatti, A. Giudice, and V. Zwiller, "Observation of strongly entangled photon pairs from a nanowire quantum dot," Nat. Commun. **5**, 5298 (2014).
18. A. Berthelot, I. Favero, G. Cassabois, C. Voisin, C. Delalande, P. Roussignol, R. Ferreira, and J.-M. Gérard, "Unconventional motional narrowing in the optical spectrum of a semiconductor quantum dot," Nat. Phys. **2**, 759–764 (2006).
19. P. Kaer, N. Gregersen, and J. Mørk, "The role of phonon scattering in the indistinguishability of photons emitted from semiconductor cavity QED systems," New J. Phys. **15**, 035027 (2013).
20. M. Munsch, A. V. Kuhlmann, D. Cadeddu, J.-M. Gérard, J. Claudon, M. Poggio, and R. J. Warburton, "Resonant driving of a single photon emitter embedded in a mechanical oscillator," Nat. Commun. **8**, 76 (2017).
21. N. Gregersen, D. P. S. McCutcheon, J. Mørk, J.-M. Gérard, and J. Claudon, "A broadband tapered nanocavity for efficient nonclassical light emission," Opt. Express **24**, 20904–20924 (2016).
22. I. Friedler, P. Lalanne, J. P. Hugonin, J. Claudon, J. M. Gérard, A. Beveratos, and I. Robert-Philip, "Efficient photonic mirrors for semiconductor nanowires," Opt. Lett. **33**, 2635–2637 (2008).
23. N. Gregersen, T. R. Nielsen, J. Mørk, J. Claudon, and J.-M. Gérard, "Designs for high-efficiency electrically pumped photonic nanowire single-photon sources," Opt. Express **18**, 21204–21218 (2010).
24. I. Friedler, C. Sauvan, J. P. Hugonin, P. Lalanne, J. Claudon, and J. M. Gérard, "Solid-state single photon sources: the nanowire antenna," Opt. Express **17**, 2095–2110 (2009).
25. J. Iles-Smith, D. P. S. McCutcheon, A. Nazir, and J. Mørk, "Phonon scattering inhibits simultaneous near-unity efficiency and indistinguishability in semiconductor single-photon sources," Nat. Photonics **11**, 521–526 (2017).
26. R. Machorro, E. Samano, G. Soto, F. Villa, and L. Cota-Araiza, "Modification of refractive index in silicon oxynitride films during deposition," Mater. Lett. **45**, 47–50 (2000).
27. T. Häyrynen, J. R. de Lasson, and N. Gregersen, "Open-geometry Fourier modal method: Modeling nanophotonic structures in infinite domains," J. Opt. Soc. Am. A **33**, 1298–1306 (2016).
28. A. V. Lavrinenko, J. Lægsgaard, N. Gregersen, F. Schmidt, and T. Søndergaard, "Numerical Methods in Photonics," (CRC Press, 2015), chap. 6, pp. 139–195.
29. M. Lermer, N. Gregersen, F. Dunzer, S. Reitzenstein, S. Höfling, J. Mørk, L. Worschech, M. Kamp, and A. Forchel, "Bloch-wave engineering of quantum dot micropillars for cavity quantum electrodynamics experiments," Phys. Rev. Lett. **108**, 057402 (2012).
30. N. Gregersen, S. Reitzenstein, C. Kistner, M. Strauss, C. Schneider, S. Höfling, L. Worschech, A. Forchel, T. R. Nielsen, J. Mørk, and J.-M. Gérard, "Numerical and experimental study of the Q factor of high-Q micropillar cavities," IEEE J. Quantum Electron. **46**, 1470–1483 (2010).
31. M. Munsch, J. Claudon, J. Bleuse, N. S. Malik, E. Dupuy, J.-M. Gérard, Y. Chen, N. Gregersen, and J. Mørk, "Linearly polarized, single-mode spontaneous emission in a photonic nanowire," Phys. Rev. Lett. **108**, 077405 (2012).
32. P. Lalanne, J. P. Hugonin, and J. M. Gérard, "Electromagnetic study of the quality factor of pillar microcavities in the small diameter limit," Appl. Phys. Lett. **84**, 4726–4728 (2004).